Simulation of Highly Nonlinear Electrokinetics Using a Weak Formulation

Gaurav Soni[†§], Todd M. Squires[¶], Carl D. Meinhart[†§]

[†]Department of Mechanical Engineering
University of California Santa Barbara, CA 93106, USA

[¶] Department of Chemical Engineering
University of California Santa Barbara, CA 93106, USA

[§] Corresponding Authors: meinhart@engr.ucsb.edu, gsoni@engr.ucsb.edu

Abstract

We present a numerical model for simulating highly nonlinear electrokinetic phenomena which happen at high zeta potentials. In this model, the electric double layer is realized by solving a partial differential equation (PDE) on the double-layer-inducing surface. This surface PDE is derived by conserving ionic charge in the double layer. A normal ohmic current and a tangential surface conduction current are both considered in the charge conservation. We also allow for a nonlinear surface capacitance, which relates the surface charge density to the zeta potential of the surface. This model is more advanced than the linear models based on Debye Huckel approximation. The linear model ignores the presence of surface conduction completely and uses a linearized surface capacitance. These simplifications are not valid for situations in which the zeta potential is much higher than the thermal voltage. With our model, we have quantified the impact of surface conduction on the magnitude of induced-charge-electroosmotic slip velocity. We predict that surface conduction significantly reduces the slip velocity and thus needs to be accounted for in all high-voltage electroosmotic simulations.

Key Words: Induced Charge Electroosmosis, Surface Conduction, Nonlinear Double Layer Capacitance

1. Introduction

In the last one decade, the research on electroosmotic phenomena has gained a lot of momentum because of their applications in 'lab on a chip' devices. A lot of practical applications have been developed which utilize electroosmotic phenomena for microscale fluid manipulation. For example, AC electroosmosis (ACEO) [1-5] has been used as a method of concentrating DNA in a micro-concentrator [6, 7]. AC electroosmosis has also been shown as a mechanism for micro pumping by introducing asymmetry in the electrode design [8-15]. Recently, it has been shown that both AC and DC electric fields can produce fluid flow on surfaces which do not necessarily have any fixed charge (unlike DC electroosmosis) or applied potential (unlike AC electroosmosis). This phenomenon has been termed induced-charge electroosmosis (ICEO) [16-19].

In addition to practical development, numerical work has also been carried out by workers for gaining better understanding of the electroosmotic phenomena. In many papers, however, the double layer has been implemented as a linear capacitor [5, 18]. The linear capacitor model results from Debye Huckel approximation which is valid only for very low zeta potentials ($\zeta \ll kT / e = 25\,\text{mVolt}$). For simulating high voltage situations accurately, we need to include nonlinear effects in the double layer models. There are several effects which might take place at high zeta potentials. Some examples include nonlinear double layer capacitance, surface conduction and faradaic reactions. The capacitance of the double layer refers to a relation between the surface charge density and the zeta potential. At high zeta potentials, the double layer behaves as a nonlinear capacitor requiring exponentially large amount of ionic charge $q \propto \sinh\left(ze\zeta / kT\right)$ [20, 21]. This means that an exponentially long time is required for charging the double layer completely. This

results in very long-time charging when using AC electric fields.

Surface conduction, on the other hand, refers to movement of ionic charge within the double layer [20]. At high zeta potentials, the conductivity of the ionic fluid close to the surface (i.e. in the double layer) might be much higher than the bulk and a significant amount of current might flow parallel to the surface through the double layer. When a lot of charge flows parallel to the surface, similarly large amount of charge has to be supplied from the bulk in form of a normal flux [22, 23]. This causes the electric field to have a large normal component and thus tangential component is reduced. This creates a deteriorating impact on the slip velocity.

In this paper, we present a numerical scheme which allows us to implement nonlinear capacitance and surface conduction. After introducing the scheme, we present the results from a DC simulation of induced charge electroosmosis on a flat metal electrode. For DC cases, the nonlinear capacitance of the double layer does not affect the slip velocity because enough time is provided for charging of the double layer. However, surface conduction can certainly take place. We have quantified the impact of surface conduction on the electroosmotic slip velocity. We predict that the deteriorating impact of surface conduction on slip velocity is significantly pronounced as zeta potential increases.

2. Induced Charge Electroosmosis
ICEO refers to a phenomenon in which a DC or AC electric field induces charge on a polarizable surface (metal or dielectric), and produces an electroosmotic slip by applying a body force on the electric double layer [16, 17]. Since the double layer is created and moved by the same electric field, this phenomenon gives rise to steady flows in both DC and AC electric fields.

Consider a flat conductor surface in contact with an electrolytic solution. When it is subjected to an external electric field $\mathbf{E} = E_0\hat{x}$ at $t = 0$, the electric field lines intersect the surface at right angles and a charge density is induced on the surface because of charge separation (figure 1a). However, the field lines start changing their

configuration as a conduction current $\mathbf{J} = \sigma\mathbf{E}$ drives positive ions towards one half of the surface ($x < 0$) and negative ions to the other half ($x > 0$). This process develops a double layer on the surface which grows as long as the normal electric field drives ions into it. In the steady state, assuming that there is no surface conduction or faradaic injection, the double layer insulates the surface completely and no electric field lines can penetrate into it. In this state, all the electric field lines are tangential to the surface (figure 1b) and cause an electroosmotic slip directed from the edges toward the center giving rise to two symmetric rolls above the surface (figure 1c). An AC field will drive an identical flow as the change in the direction of the field changes the polarity of the induced charge as well.
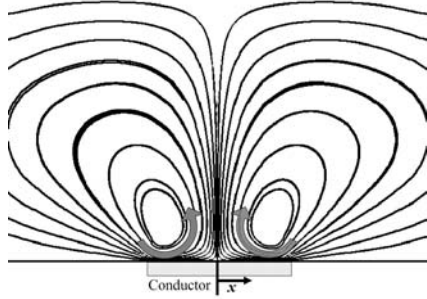

(a) *t=0*

(b) Steady state

(c) ICEO flow
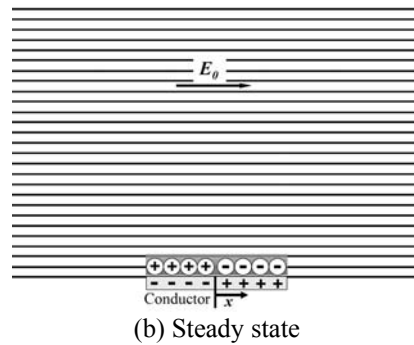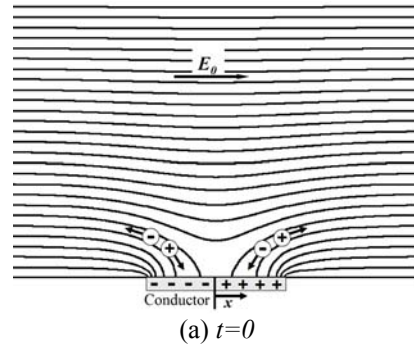
Figure 1: Induced charge electroosmosis on a conducting surface. (a) At time t=0, there is no double layer, hence all the field lines are perpendicular to the surface, (b) In the steady state, double layer gets completely charged and all the field lines become tangential to the surface, (c) The tangential field causes the double layer to move and produces symmetric ICEO flow.

The slip velocity u_{slip} is given by the Helmholtz Smoluchowski equation,

$$u_{slip} = -\frac{\varepsilon}{\eta}\zeta E_t ,$$ (1)

where ε and η are respectively the absolute permittivity and viscosity of the ionic solution, ζ is zeta potential of the surface and E_t is the electric field component tangential to the surface. ζ is defined as the potential drop across the diffuse part of the double layer. One can note that in an ideal case where the double layer gets fully charged and there is no stern layer or surface conduction present, $E_t = E_0$ and $\zeta = E_0 x$. By substituting these in (1), we get

$$u_{slip} = -\frac{\varepsilon E_0^2}{\eta}x .$$ (2)

This shows that the velocity is symmetric about $x = 0$ and the maximum slip velocity occurs at the left and right edges of the surface.

3. Capacitance of the Double Layer
The double layer capacitance is the ratio of the charge in the double layer to the voltage drop across it. When no assumption of linearity is made, the surface charge density of the ionic

charge in the double layer, q (C m^{-2}) is given by [21],

$$q = -\frac{\varepsilon}{\lambda_D}\frac{2kT}{ze}\sinh\left(\frac{ze\zeta}{2kT}\right).$$ (3)

4. Surface conduction
The surface current is dependent on the surface conductivity of the double layer and can be expressed as follows,

$$j_s = \sigma_s \mathbf{E}_t .$$ (4)

where j_s is the excess surface current density per unit width in C s^{-1} m^{-1} = A m^{-1}, σ_s is the excess surface conductivity in A V^{-1} = Siemen and $\mathbf{E}_t$ is the tangential electric field causing the current.

4.1 Surface Conductivity of the Diffuse Layer
Following the analysis by Lyklema 2001 [20], the surface conductivity for a symmetric electrolyte (with $z_+ = z_- = z$ and $D_+ = D_- = D$) can be expressed as

$$\sigma_s = 4\lambda_D \sigma (1+m)\sinh^2\left(\frac{ze\zeta}{4kT}\right),$$ (5)

where σ is the bulk conductivity and

$$m = 2\frac{\varepsilon}{\eta D}\left(\frac{kT}{ze}\right)^2 .$$ (6)

is a dimensionless parameter indicating the relative contribution of electroosmosis to surface conduction.

4.2 Dukhin Number
Usually, the surface conductivity is expressed in terms of a dimensionless parameter, Dukhin number Du, defined as.

$$Du = \frac{\sigma_s}{\sigma a},$$ (7)

where a is the characteristic length scale. Combining equations (5) and (7) we get

$$Du = \frac{4\lambda_D}{a}(1+m)\sinh^2\left(\frac{ze\zeta}{4kT}\right). \qquad (8)$$

The preceding equation for Dukhin number accounts only for diffuse layer surface conduction. We have not accounted for the stern layer surface conduction because the ionic mobility and diffusivity in the stern layer are unknown. Strategies to estimate the stern layer are enumerated in [20].

5. Charge Conservation in the Double Layer

Assuming that the double layer is infinitely thin ($\lambda_D/a \ll 1$) and double layer charging does not create any gradients in the bulk electrolyte concentration, the charge conservation equation for the surface charge density in the double layer is expressed as

$$\frac{\partial q}{\partial t} = \hat{n}\cdot(\sigma\nabla\phi) + \nabla_t\cdot(\sigma_s\nabla_t\phi), \qquad (9)$$

where ϕ is electrostatic potential outside the double layer and ∇_t is the tangential gradient operator on the outer surface of the double layer and $\hat{n}$ is the normal vector. The first term on the right signifies the normal ohmic flux whereas the second surface conduction flux. If the electrode surface lies in the *x-y* plane, then the tangential gradient operator is simply $\nabla_t = \hat{i}\,\partial/\partial x + \hat{j}\,\partial/\partial y$.

5.1. Condition on the Edges of the Electrode

Since we are solving a PDE (equation (9)) on the electrode surface, we need to provide conditions on the boundaries (i.e. the edges) of the electrode. To define a condition, we take the surface conduction flux to be zero at the edges, i.e.,

$$\hat{s}\cdot(\sigma_s\nabla_t\phi) = 0, \qquad (10)$$

where $\hat{s}$ is a vector which is tangential to the surface but perpendicular to the edge of the electrode. Surface conduction is zero at the edges because all electric field lines at the edges are perpendicular and there is no tangential field to drive the surface current.

5.2. Convergence Issues

Equation (9) solves for double layer surface charge density *q* because the time derivative of *q* occurs on the left hand side. However, the spatial terms on the right hand side do not contain *q*. These terms depend on the bulk potential ϕ and therefore behave as sources. Essentially, there is no diffusive term available for *q* in the equation for *q*. The absence of diffusive terms combined with the presence of source terms leads to an infinite Péclet number and can create convergence problems. Moreover, magnitude of *q* is supposed to grow exponentially as predicted by equation (3); this means that the computer will solve for a variable which is very large. This will lead to large numerical errors.

In order to alleviate the aforementioned problems with the PDE in *q*, we will transform the dependent variable *q* into ζ. By differentiating (3) with respect to time, we can obtain an expression for $\partial q/\partial t$ in terms of $\partial\zeta/\partial t$,

$$\frac{\partial q}{\partial t} = -\frac{\varepsilon}{\lambda_D}\cosh\left(\frac{ze\zeta}{2kT}\right)\frac{\partial\zeta}{\partial t}. \qquad (11)$$

Similarly by using the relation $\phi = \phi_{el} - \zeta$, where ϕ_{el} is the potential applied to the electrode and ignoring the stern layer, we can obtain an expression for the tangential divergence in terms of ζ

$$\nabla_t\cdot(\sigma_s\nabla_t\phi) = -\nabla_t\cdot(\sigma_s\nabla_t\zeta). \qquad (12)$$

Combining the two preceding equations with equation (9) we get

$$\frac{\partial\zeta}{\partial t} = -\frac{\lambda_D\left[\hat{n}\cdot(\sigma\nabla\phi) - \nabla_t\cdot(\sigma_s\nabla_t\zeta)\right]}{\varepsilon\cosh\left(ze\zeta/2kT\right)}. \qquad (13)$$

Using the definitions $\tau_c = \varepsilon a/\sigma\lambda_D$ and $Du = \sigma_s/\sigma a$, the preceding equation reduces to

$$\tau_C\frac{\partial\zeta}{\partial t} = -\frac{\left[a\hat{n}\cdot\nabla\phi - a^2\nabla_t\cdot(Du\nabla_t\zeta)\right]}{\cosh\left(ze\zeta/2kT\right)}, \qquad (14)$$

which is a well behaved equation in ζ. The first term on the right hand side ($a\hat{n} \cdot \nabla \phi$) is supplied from the bulk and behaves as a source. The second term on the right behaves as a diffusion term in ζ.

Another advantage of changing the dependent variable from q to ζ is that it produces a factor of $1/\cosh\left(ze\zeta/2kT\right)$ on the right hand side; in other words, the right hand side is divided by a large number and thus the solution consists of numbers with small magnitudes; this makes the problem easier to converge. Another way of understanding the variable substitution is the following: magnitudes of ζ are generally much smaller than q (see nonlinear capacitance equation (3)); hence we prefer to solve for ζ instead of q.

When one wants to solve for a steady state, equation (14) is reduced to

$$\hat{n} \cdot \nabla \phi - a\nabla_t \cdot (Du\nabla_t \zeta) = 0 . \qquad (15)$$

6. Dimensionless Equations

In most of the situations, following scales will be appropriate for making the equations dimensionless. Asterisk in the superscript represents a dimensionless quantity.

$$\begin{aligned}
\mathbf{x} &= a\mathbf{x}^* , \\
\phi &= \phi_0 \phi^* , \\
q &= q^* \varepsilon\phi_0/\lambda_D , \\
t &= \tau_C t^* , \\
\mathbf{u} &= u_{HS}\mathbf{u}^* , \\
p &= p^* \eta u_{HS}/a ,
\end{aligned} \qquad (16)$$

where, $\phi_0 = kT/ze$ is the thermal voltage and u_{HS} is an appropriate scale for the Helmholtz Smoluchowski velocity; u_{HS} can be chosen based on geometry and application.

The dimensionless charge conservation equation is then expressed as

$$\frac{\partial \zeta^*}{\partial t^*} = -\frac{\left[\hat{n} \cdot \nabla^* \phi^* - \nabla_t^* \cdot (Du\nabla_t^* \zeta^*)\right]}{\cosh\left(\zeta^*/2\right)} . \qquad (17)$$

For a steady state, equation (17) simplifies to

$$\hat{n} \cdot \nabla^* \phi^* - \nabla_t^* \cdot (Du\nabla_t^* \zeta^*) = 0 . \qquad (18)$$

The edge conditions in form of dimensionless variables are given as

$$\hat{s} \cdot (Du\nabla_t^* \zeta^*) = 0 . \qquad (19)$$

Dukhin number can also be expressed in terms of dimensionless variables,

$$Du = 4\lambda^* \left(1+m\right)\sinh^2\left(\zeta^*/4\right) , \qquad (20)$$

where λ^* is the dimensionless double layer thickness, $\lambda^* = \lambda_D/a$. Similarly, the nonlinear capacitive relation reduces to

$$q = -2\sinh\left(\zeta^*/2\right) . \qquad (21)$$

The dimensionless equations for the bulk can be written as

$$\nabla^{*2}\phi^* = 0 , \qquad (22)$$

$$\mathrm{Re}\,\mathbf{u}^* \cdot \nabla^* \mathbf{u}^* = -\nabla^* p^* + \nabla^{*2}\mathbf{u}^* , \qquad (23)$$

$$\nabla^* \cdot \mathbf{u}^* = 0 , \qquad (24)$$

where $\mathrm{Re} = \rho u_{HS} a/\eta$ is the Reynolds numbers. In most of microfluidic situations, $\mathrm{Re} \ll 1$.

The boundary conditions for the walls are

$$\hat{n} \cdot \nabla^* \phi^* = 0 , \qquad (25)$$

and

$$\mathbf{u}^* = 0 . \qquad (26)$$

At the electrodes where electroosmotic slip occurs

$$\phi^* = \phi_{el}^* - \zeta^* , \qquad (27)$$

and

$$\mathbf{u}^* = \frac{\varepsilon \phi_0^2/a\eta}{u_{HS}} \zeta^* \left(\nabla^* \phi^* \cdot \hat{t} \right) \hat{t} \ . \qquad (28)$$

where $\hat{t}$ is the tangential vector.

7. ICEO on a Flat Electrode

Consider a horizontal electrode of width a placed at the bottom wall of a chamber of side L. The chamber side is much larger than the width of the electrode, $L^*=L/a=15$ (figure 2). We will refer to the horizontal electrode as a gate electrode. The two vertical sides of the chamber serve as a pair of driving electrodes; a DC electric field is produced in the chamber by applying a potential difference between the two driving (vertical) electrodes. The chamber is filled with a symmetric ($z_+ = z_- = z$ and $D_+ = D_- = D$) electrolyte solution such as $KCl+H_2O$. Assume that the driving electrodes do not saturate (i.e. no double layer) and can maintain a constant DC electric field in the chamber. Equal and opposite potentials are applied to the two driving electrodes; the gate electrode is kept floating; the floating potential on the gate vanishes i.e. $\phi_{el}^* = 0$ because it is placed at equal distances from the two driving electrodes. One consequence of zero floating potential is that the bulk boundary condition becomes $\phi^* = -\zeta^*$.
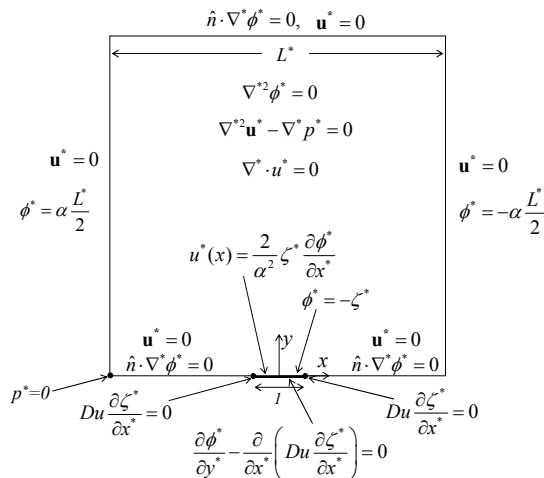

$$\hat{n}\cdot\nabla^*\phi^* = 0, \quad \mathbf{u}^* = 0$$

$$\nabla^{*2}\phi^* = 0$$

$$\nabla^{*2}\mathbf{u}^* - \nabla^* p^* = 0$$

$$\nabla^* \cdot u^* = 0$$

$$\mathbf{u}^* = 0 \qquad \mathbf{u}^* = 0$$

$$\phi^* = \alpha\frac{L^*}{2} \qquad \phi^* = -\alpha\frac{L^*}{2}$$

$$u^*(x) = \frac{2}{\alpha^2}\zeta^*\frac{\partial \phi^*}{\partial x^*}$$

$$\phi^* = -\zeta^*$$

$$\mathbf{u}^* = 0 \qquad \mathbf{u}^* = 0$$
$$\hat{n}\cdot\nabla^*\phi^* = 0 \qquad \hat{n}\cdot\nabla^*\phi^* = 0$$

$$p^* = 0$$
$$Du\frac{\partial \zeta^*}{\partial x^*} = 0 \qquad Du\frac{\partial \zeta^*}{\partial x^*} = 0$$

$$\frac{\partial \phi^*}{\partial y^*} - \frac{\partial}{\partial x^*}\left(Du\frac{\partial \zeta^*}{\partial x^*}\right) = 0$$

Figure 2: Steady state simulation model for ICEO flow on a flat electrode with $L/a=15$. Geometry is not shown to scale.

As described in section 2, symmetric ICEO flow is produced on the gate electrode as a result of the electric field [19]. Assume that the depth of the chamber into the paper is infinite. Therefore, only a 2D model needs to be simulated. Simplified steady state dimensionless equations and boundary conditions for 2D are shown on figure 2.

As shown in figure 2, the dimensionless potentials applied to the driving electrodes are $\phi^* = \pm\alpha L^*/2$. Here α is a dimensionless parameter and controls the magnitude of applied voltage signal. By design, α is a direct measure of the zeta potential induced on the gate electrode. Consider an ideal case in which there is no stern layer, no surface conduction and no faradaic injections. In the steady state, the double layer will get completely charged and the bulk potential will drop linearly from $+\alpha L^*/2$ to $-\alpha L^*/2$ across the chamber. The net drop across the length of the gate will then be α and thus the dimensionless maximum induced zeta potential will be equal to $\alpha/2$. As α grows, both ζ^* and Dukhin number grow and thus surface conduction becomes important.

Similarly, dimensionless double layer thickness $\lambda^* = \lambda_D/a$ also controls the magnitude of Dukhin number (equation (20)). We will vary both α and λ^* to quantify the impact of surface conduction on slip velocity.

Since the linear theory based zeta potential on the gate is of the order $\alpha\phi_0/2$ and the tangential electric field is approximately $\alpha\phi_0/a$, a natural scale for the slip velocity would be

$$u_{HS} = \varepsilon\alpha^2\phi_0^2/2\eta\,a \ . \qquad (29)$$

Using this scale, we can define the dimensionless (or normalized) slip velocity on the gate as

$$u^*(x) = \frac{1}{u_{HS}}\frac{\varepsilon}{\eta}\zeta\frac{\partial \phi}{\partial x} = \frac{2}{\alpha^2}\zeta^*\frac{\partial \phi^*}{\partial x^*} \ . \qquad (30)$$

7.1. Results and Discussion

The problem was solved with COMSOL Multiphysics (Comsol Inc., Stockholm, Se), a commercial finite element software package. Let's first consider a case of very thin double layer and small induced zeta potential, namely $\lambda^* = 10^{-4}$ and $\alpha = 0.1$. In this case we expect surface conduction to be negligible. In the steady state the double layer gets completely charged and electric field lines become completely tangential to the electrode (figure 3a). The normal component of the electric field is uniformly zero on the electrode. This picture is very similar to the one discussed in section 2 (figure 1(b)).

However, when α and λ^* are large ($\alpha = 31.6$, $\lambda^* = 0.01$), the steady state configuration of electric field lines is quite different (figure 3b). In this case, the electric field lines have a large normal component on the entire electrode surface, especially close to the edges. This leads to loss of tangential electric field and consequently to loss of slip velocity (figure 4).
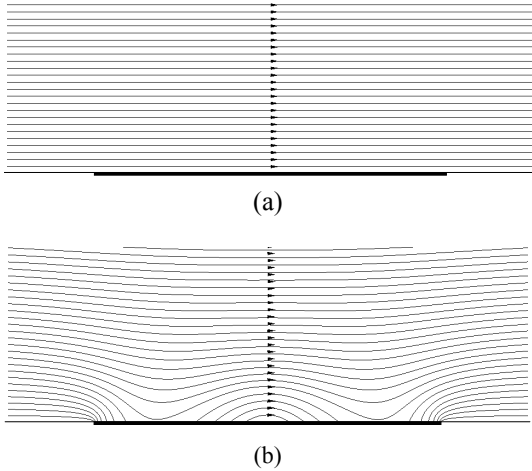

(a)

(b)

Figure 3: Steady state electric field lines in the vicinity of a flat electrode subjected to a DC electric field directed from left to write. Arrows indicate the direction of the electric field. *(a)* For very thin double layer and very low induced zeta potential (i.e. $\lambda^* = 10^{-4}$ and $\alpha = 0.1$), the electric field is completely tangential to the electrode. *(b)* For a thick double layer and large induced zeta potential ($\lambda^* = 0.01$, $\alpha = 31.6$), surface conduction become important. The normal component of the electric field

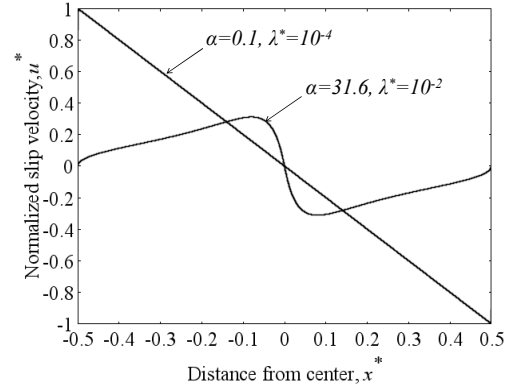becomes large so that ions can be supplied for the surface conduction current.

Figure 4: Steady state slip velocity on the gate electrode. Two cases are shown, (1) $\lambda^* = 10^{-4}$ and $\alpha = 0.1$ (2) $\lambda^* = 0.01$, $\alpha = 31.6$). In the first case, the normalized slip velocity is much higher than the second case. The loss in velocity in the second case is due to surface conduction which becomes prominent at high zeta potential (i.e. large α) and in thick double layers (i.e. large λ^*).

The peculiar pattern of the electric field lines in figure 3b can be explained by considering the surface conduction flux. Positive ions enter into the double layer in the vicinity of the left edge. Then they move parallel to the surface due to the tangential component of the electric field. However, the surface conduction flux $Du \, \partial \zeta^* / \partial x^*$ is zero at the center of the gate because ζ^* and therefore Du is zero at that location (see figures 5, 6 and 7). Hence, the center of the gate acts like a barrier for the surface current. Therefore the ions start leaking out of the double layer into the bulk. That's why the normal component of the electric field reverses direction at a point between the edge and the center (figure 8). The same occurs with negative ions on the other side of the electrode. However, this behavior can only be seen in symmetric ICEO flows. Khair and Squires 2008 [22] have discussed surface conduction on a plate with constant zeta potential. They also predict large normal component of the electric field close to the edge of the plate; however since the zeta potential is uniform, there is no conduction barrier in the middle of the plate and thus electric field lines become tangential to the plate after a healing region near the edges.
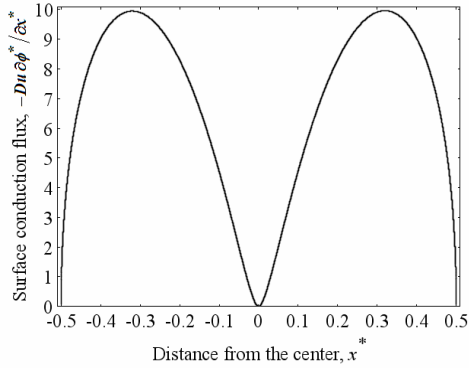
Figure 5: Steady state surface conduction flux $Du\, \partial\zeta^*/\partial x^*$ on the gate electrode for $\lambda^* = 0.01$, $\alpha = 31.6$.
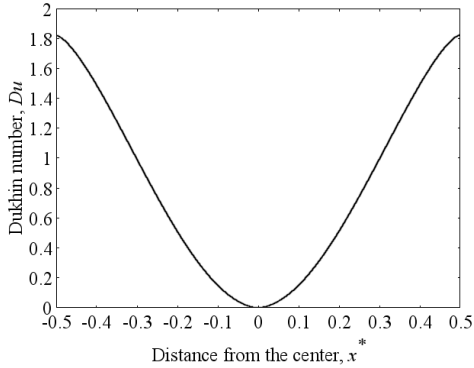

Figure 6: Steady state Dukhin number on the gate electrode for $\lambda^* = 0.01$, $\alpha = 31.6$.
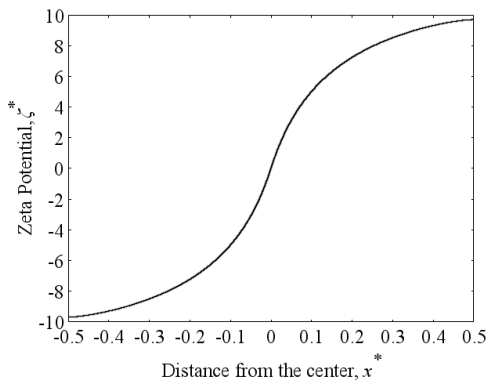

Figure 7: Steady state zeta potential ζ^* on the gate electrode for $\lambda^* = 0.01$, $\alpha = 31.6$.
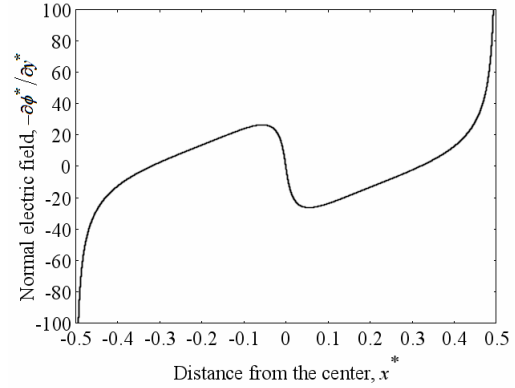

Figure 8: Steady state normal component of the electric field on the gate electrode for $\lambda^* = 0.01$, $\alpha = 31.6$. On the edges, the normal electric field is very large; here we have shown the values between -100 and 100 only.

8. Conclusions

A numerical scheme for simulating nonlinear electrokinetics has been presented. In this scheme, the electric double layer is handled by solving a charge-conservation PDE on the electrode surface. A variable substitution is proposed for improving the convergence of the model. The new model has excellent convergence properties and has been used for solving electrokinetic problems for very high induced zeta potentials (about 15 times higher than the thermal voltage). The model allows for nonlinear effects such as nonlinear capacitance and surface conduction. We have portrayed both qualitative and quantitative pictures of surface conduction and its impact on ICEO flows. We predict that surface conduction creates large normal electric fields and thus reduces the tangential field as well as the slip velocity significantly.

APPENDIX
Use of COMSOL Multiphysics

A commercial finite element package COMSOL Multiphysics (Comsol Inc., Stockholm, Sweden) was used for solving the mathematical model described in this paper. Lagrange quadratic elements were used for all the dependent variables. Since the problem deals with DC electric fields, a stationery solver was used with zero initial conditions for all the variables. A Direct (UMFPACK) solver was chosen for solving the system of linear equations. First the

electrostatics and double layer PDE were solved simultaneously. Then their solution was used as a linearization point for the bulk fluid flow problem. The mesh element size on the ICEO electrode boundary was one hundredth of the dimensionless double layer thickness λ^* so that a mesh independent solution can be achieved. For example, if $\lambda^* = 0.01$, the maximum element size on the electrode would be 1E-4. However, it wasn't possible to have an element size of $\lambda^*/100$ for very low values of λ^* (such as $\lambda^* = 10^{-4}$). In such cases, the element size close to the edges was chosen to be $\lambda^*/100$. Weak constraints were used for handling the dirichlet boundary conditions. Important details about the weak constraints are shown in table 1.

Weak Form

Finite element methods generally seek a weak solution to the PDE in question. As an example consider Poisson equation,

$$\nabla^2 u(\mathbf{x}) = f(\mathbf{x}), \quad \mathbf{x} \in \Omega \quad (31)$$

Suppose H is an infinite-dimensional function space that is rich enough to include in its closure all functions that may be of interest as candidates for the solution u. For all $v \in H$, we define the defect $d(v) = \nabla^2 v - f$. Then we say that w is a *weak solution* to the problem equation (31) provided that the defect $d(w)$ is orthogonal to the entire function space, that is, if

$$\int_\Omega v d(w) d\mathbf{x} = 0 \quad \forall v \in H. \quad (32)$$

v is generally referred to as a *test function*. Equation (32) is also referred as the *weak form* of equation (31). For more information, the reader is referred to [24, 25].

We can further simplify equation (32) as

$$\int_\Omega v \nabla^2 w d\mathbf{x} - \int_\Omega v f d\mathbf{x} = 0. \quad (33).$$

The first term on right hand can be simplified to

$$\int_\Omega v \nabla^2 w d\mathbf{x} = \int_\Omega \nabla \cdot (v \nabla w) d\mathbf{x} - \int_\Omega \nabla v \cdot \nabla w d\mathbf{x}. (34)$$

Applying divergence theorem on the first term on the right hand side yields

$$\int_\Omega v \nabla^2 w d\mathbf{x} = \int_{\partial\Omega} v \hat{n} \cdot \nabla w d\mathbf{s} - \int_\Omega \nabla v \cdot \nabla w d\mathbf{x}, (35)$$

where $\partial\Omega$ is the boundary of Ω. The boundary integrals can be handled by invoking the boundary conditions. For example, if a Neumann boundary condition is specified on the boundary, i.e., $\hat{n} \cdot \nabla w = b(x)$, then we can simply substitute it in the boundary integral. Dirichlet conditions are handled by implementing constraints [25].

Weak Form of the Double Layer PDE

To implement the charge conservation equation in COMSOL, it's necessary to derive its weak form. When doing a steady state analysis, one has to solve equation (18) on the surface. Following the procedure described in the previous section, the weak form of equation (18) is simply given as

$$\int_S v \hat{n} \cdot \nabla^* \phi^* d\mathbf{s} - \int_S Du \nabla_t^* v \cdot \nabla_t^* \zeta^* d\mathbf{s} = 0 \quad (36)$$

where S represents the surface and v is a test function for ζ^*. Note that the edge condition $\hat{s} \cdot (Du \nabla_t^* \zeta^*) = 0$ was invoked in derivation of equation (36).

For a time dependent analysis, however, the weak form of equation (17) is expressed as

$$\int_S v \frac{\partial \zeta^*}{\partial t^*} d\mathbf{s} = -\int_S v \frac{\hat{n} \cdot \nabla^* \phi^* - \nabla_t^* \cdot (Du \nabla_t^* \zeta^*)}{\cosh(\zeta^*/2)} d\mathbf{s}. (37)$$

The second term on the right hand side can be expanded as follows

$$\int_S v \frac{\nabla_t^* \cdot (Du\nabla_t^*\zeta^*)}{\cosh(\zeta^*/2)} d\mathbf{s} =$$

$$\int_S \nabla_t^* \cdot \left(\frac{v}{\cosh(\zeta^*/2)} Du\nabla_t^*\zeta^* \right) d\mathbf{s}$$

$$-\int_S Du \frac{\left[\nabla_t^* v \cdot \nabla_t^*\zeta^* - \frac{v}{2}\tanh(\zeta^*/2)\nabla_t^*\zeta^* \cdot \nabla_t^*\zeta^* \right]}{\cosh(\zeta^*/2)} d\mathbf{s}$$

$$.(38)$$

The first term on the right hand side of the preceding equation can be simplified by applying the divergence theorem

$$\int_S \nabla_t^* \cdot \left(\frac{v}{\cosh(\zeta^*/2)} Du\nabla_t^*\zeta^* \right) d\mathbf{s} =$$

$$\int_{Edges} \frac{vDu}{\cosh(\zeta^*/2)} \hat{s} \cdot \nabla_t^*\zeta^* d\mathbf{l} \qquad (39)$$

However, we have $\hat{s} \cdot \nabla_t^*\zeta^* = 0$ on the edges and therefore

$$\int_S \nabla_t^* \cdot \left(\frac{v}{\cosh(\zeta^*/2)} Du\nabla_t^*\zeta^* \right) d\mathbf{s} = 0 . \qquad (40)$$

Finally combining equations (38) and (40) with equation (37) yields

$$\int_S v \frac{\partial \zeta^*}{\partial t^*} d\mathbf{s} =$$

$$-\int_S \frac{v\hat{n} \cdot \nabla^*\phi^*}{\cosh(\zeta^*/2)} d\mathbf{s}$$

$$-\int_S \frac{Du\left[\nabla_t^*\zeta^* \cdot \nabla_t^* v - \frac{v}{2}\tanh(\zeta^*/2)\nabla_t^*\zeta^* \cdot \nabla_t^*\zeta^* \right]}{\cosh(\zeta^*/2)} d\mathbf{s}$$

$$. (41)$$

Table 1: Comments on weak constraints

Equation	COMSOL Mode	Weak Constraints	Comments
Laplace's equation	Electrostatics	Ideal	The electrostatics problem is coupled to the double layer PDE through a dirichlet b.c. on the ICEO electrode. This coupling can be handled by either weak ideal or weak non-ideal constraints. The results depend upon the choice of weak constraints; both choices capture the essential physics behind surface conduction and predict similar trends. We have chosen the ideal weak constraints.
Double layer charge conservation	PDE Mode, Weak Form, Boundary	off	There is no dirichlet condition in this mode so weak constraints are not required.
Bulk fluid flow	Incompressible Navier-Stokes	Non-ideal	Slip b.c. on the ICEO electrode represents a constraint. Weak non-ideal constraints are required for decoupling the electrostatics problem from fluid flow problem.

REFERENCES:

1. Ramos, A., et al., *Ac electrokinetics: a review of forces in microelectrode structures.* Journal of Physics D-Applied Physics, 1998. **31**(18): p. 2338-2353.

2. Ramos, A., et al., *AC electric-field-induced fluid flow in microelectrodes.* Journal of Colloid and Interface Science, 1999. **217**(2): p. 420-422.

3. Green, N.G., et al., *Fluid flow induced by nonuniform ac electric fields in electrolytes*

on microelectrodes. I. Experimental measurements. Physical Review E, 2000. **61**(4): p. 4011-4018.

4. Gonzalez, A., et al., *Fluid flow induced by nonuniform ac electric fields in electrolytes on microelectrodes. II. A linear double-layer analysis.* Physical Review E, 2000. **61**(4): p. 4019-4028.

5. Green, N.G., et al., *Fluid flow induced by nonuniform ac electric fields in electrolytes on microelectrodes. III. Observation of streamlines and numerical simulation.* Physical Review E, 2002. **66**(2): p. 11.

6. Wong, P.K., et al., *Electrokinetic bioprocessor for concentrating cells and molecules.* Analytical Chemistry, 2004. **76**(23): p. 6908-6914.

7. Bown, M.R. and C.D. Meinhart, *AC electroosmotic flow in a DNA concentrator.* Microfluidics and Nanofluidics, 2006. **2**(6): p. 513-523.

8. Ajdari, A., *Pumping liquids using asymmetric electrode arrays.* Physical Review E, 2000. **61**(1): p. R45-R48.

9. Ramos, A., et al., *Pumping of liquids with ac voltages applied to asymmetric pairs of microelectrodes.* Physical Review E, 2003. **67**(5): p. 11.

10. Seibel, K., et al. *Transport properties of ac electroosmotic micropumps on labchips.* 2003. Cambridge, UK.

11. Ramos, A., et al., *Pumping of electrolytes using arrays of asymmetric pairs of microelectrodes subjected to ac voltages*, in *Electrostatics 2003*. 2004, Iop Publishing Ltd: Bristol. p. 187-192.

12. Studer, V., et al., *An integrated AC electrokinetic pump in a microfluidic loop for fast and tunable flow control.* Analyst, 2004. **129**(10): p. 944-949.

13. Garcia-Sanchez, P., et al., *Experiments on AC electrokinetic pumping of liquids using arrays of microelectrodes.* Ieee Transactions on Dielectrics and Electrical Insulation, 2006. **13**(3): p. 670-677.

14. Olesen, L.H., H. Bruus, and A. Ajdari, *ac electrokinetic micropumps: The effect of geometrical confinement, Faradaic current injection, and nonlinear surface capacitance.* Physical Review E, 2006. **73**(5).

15. Ramos, A., et al., *Pumping of liquids with traveling-wave electroosmosis.* Journal of Applied Physics, 2005. **97**(8): p. 8.

16. Squires, T.M. and M.Z. Bazant, *Induced-charge electro-osmosis.* Journal of Fluid Mechanics, 2004. **509**: p. 217-252.

17. Bazant, M.Z. and T.M. Squires, *Induced-charge electrokinetic phenomena: Theory and microfluidic applications.* Physical Review Letters, 2004. **92**(6): p. 4.

18. Levitan, J.A., et al., *Experimental observation of induced-charge electro-osmosis around a metal wire in a microchannel.* Colloids and Surfaces a-Physicochemical and Engineering Aspects, 2005. **267**(1-3): p. 122-132.

19. Soni, G., Squires, T.M., Meinhart, C.D., *Nonlinear Phenomena in Induced Charge Electroosmosis.* Proceedings of 2007 ASME International Mechanical Engineering Congress and Exposition, Seattle, Washington, 2007: p. IMECE2007-41468.

20. Lyklema, J., *Fundamentals of interface and colloid science, Volume II: Solid-liquid interfaces.* 2001: Academic press.

21. Bard, A.J. and L.R. Faulkner, *Electrochemical methods, Fundamentals and applications.* second ed. 2001: John Wiley & Sons, Inc.

22. Khair, A.S. and T.M. Squires, *Surprising consequences of ion conservation in electro-osmosis over a surface charge discontinuity.* Under consideration for publication in J. Fluid Mech., 2008.

23. Khair, A.S. and T.M. Squires, *Fundamental aspects of concentration polarization arising from nonuniform electrokinetic transport.* Physics of Fluids, 2008. **20**: p. 087102.

24. Johnson, C., *Numerical solution of partial differential equations by the finite element method.* Studentlitteratur/Cambridge University Press, 1987.

25. Olesen, L.H., *Computational Fluid Dynamics in Microfluidic Systems* Master Thesis, Technical University of Denmark, Denmark., 2003.